AIAA 2000-3753
Particle Simulations of Plasma Heating in VASIMR

A.V. Ilin, F.R. Chang Díaz, J.P. Squire,
ASPL, JSC / NASA, Houston, TX,

B.N. Breizman,
UT, Austin, TX,

M.D. Carter,
ORNL, Oak Ridge, TN

36th AIAA/ASME/SAE/ASEE
Joint Propulsion Conference
17-19 July 2000
Huntsville, Alabama

PARTICLE SIMULATIONS OF PLASMA HEATING IN VASIMR

Andrew V. Ilin*, Franklin R. Chang Díaz†, Jared P. Squire‡,
Advanced Space Propulsion Laboratory, JSC / NASA, Houston, TX,
Boris N. Breizman§, University of Texas at Austin, Austin, TX,
and Mark D. Carter¶, Oak Ridge National Laboratory, Oak Ridge, TN

ABSTRACT

An important motivation for particle simulation in a Variable Specific Impulse Magnetoplasma Rocket (VASIMR) is plasma heating by Radio Frequency (RF) electromagnetic waves. Mathematical simulation helps with the design of an Ion-Cyclotron Radio Frequency (ICRF) antenna by showing where adjustments can maximize the power coupling and control the absorption profile of RF power into the plasma in the resonance area. Not only should the ions gain high energy from the ICRF waves, but the heating must also be accompanied by a high antenna loading to reduce power loss in the RF circuit.

INTRODUCTION

Progress toward a reasonably self-consistent mathematical model in a Variable Specific Impulse Magnetoplasma Rocket (VASIMR)[1,2,3] is examined. The goal of this modeling is to help understand the physics of the system behavior at the Advanced Space Propulsion Laboratory and to assist engineers in the design of a thruster suitable for flight testing.

Computer simulation of plasmas are typically be done by using one of, or a combination of three general techniques: a fluid approximation, Vlasov / Fokker-Planck models, and full particle descriptions. The particle methods can give much more accurate results when fully kinetic descriptions are needed in systems where collisions may also be important. Such systems include those with strong, resonant Radio Frequency (RF) ion heating, collision events resulting in large phase space changes for the particles and other non-thermal effects, and for magnetic shielding of structures from the solar flare among others.

Although particle codes require much more computational resources than other plasma simulation techniques, rapid growth in computer speed and memory in the last few years has made the particle description more tractable.[4] The particle methods, presented by Particle-in-Cell (PIC) and direct simulation Monte-Carlo (DSMC) methods, are efficiently used for simulation of the Pulsed Plasma Thruster (PPT)[5], the Hall Thruster[6] as well as the Ion Thruster[7]. In this paper we use a particle method, which is called a trajectory method[8], and combine it with other modeling techniques to produce a reasonably self-consistent model for the entire VASIMR system.

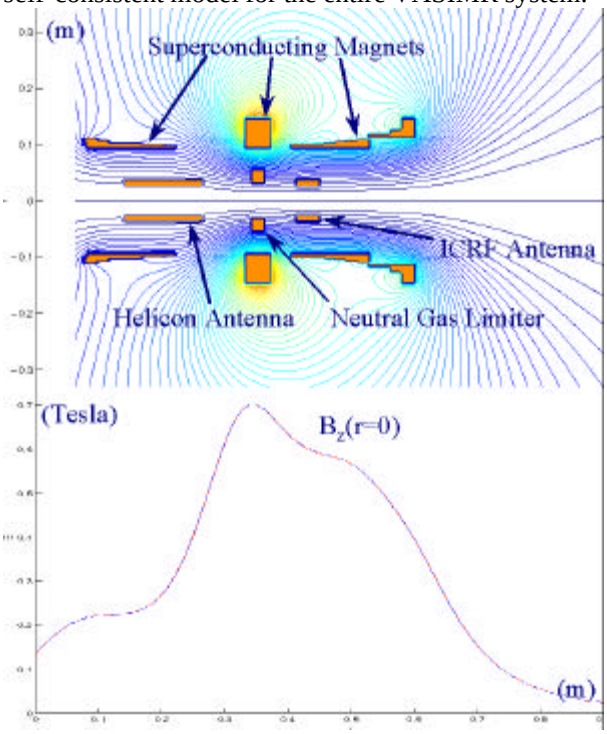

Figure 1. Geometry and magnetic field configuration for VASIMR.

* Research Scientist, Muniz Engineering Inc.
ilin@jsc.nasa.gov
† NASA Astronaut, ASPL Director
‡ Senior Research Scientist, Muniz Engineering Inc.
§ Research Scientist, Institute for Fusion Studies
¶ Research Staff, Fusion Energy Division

The VASIMR system consists of three major magnetic cells, denoted as "forward," "central," and "aft". [1,2,3] An example of electromagnets with their corresponding magnetic field is demonstrated in Figure 1.

The forward end-cell provides for the injection of gas to be ionized into the plasma state; in this case by electromagnetic waves that are produced by the helicon antenna. The central-cell acts as an amplifier and serves to further heat the ions in the plasma by electromagnetic waves produced by an antenna operating near the Ion-Cyclotron Radio Frequency (ICRF). The aft end-cell ensures that the plasma will efficiently detach from the magnetic field to provide a highly directed exhaust stream with high and variable specific impulse. This configuration allows the plasma exhaust to be guided and controlled over a wide range of plasma energies and densities.

The choice of the modeling system here is made on the basis of the expected operational requirements for a flight system. Currently, the VASIMR system is under development for a first space flight experiment using 10 kW of DC electric power. In the future, several megawatt VASIMR thrusters can be considered for human interplanetary flights to Mars and beyond[8]. The typical values of operational parameters are presented in the Table 1.

			Low Power		High Power
Power	$P_{in} = \dot{m}u^2/(2e)$	(Watt)	10^4		$> 10^7$
Mass	M	(kg)	20 - 50		< 20000
Temperature	T_e	(eV)	5 - 50		10 - 100
	T_i	(eV)	100		10 - 1000
Density	n	(m^3)	10^{18} - 10^{19}		10^{19} - 10^{21}
Mag. Field	B	(Tesla)	< 1		< 3
Plasma radius	r_p	(m)	0.025		0.1
Plasma length	L	(m)	0.5		0.5 - 1
Specific impulse	$I_{sp} = u/g$	(sec)	5000(He), 10^4(H)	3000	To 30000
Propel. flow rate	$\dot{m}$	(mg/s)	4(He), 1(H)	10^4	® 10^2
Thrust	$F = \dot{m}u$	(N)	0.2(He), 0.1(H)	> 300	® > 30
Exhaust velocity	u	(m/s)	$5 \cdot 10^4$(He), 10^5(H)	3 x 10^4	® 3 x 10^5
Efficiency	$e = P_{thrust}/P_{in}$		» 0.5	> 0.5	
Propellant species			He, H	H, He, Li, NH_3, CH_4,Xe, others	

Table 1. Typical values of the VASIMR operating parameters

This paper concerns the modeling of a low power VASIMR thruster.

MATHEMATICAL MODEL

The magnetic field in the VASIMR is a sum of the fields generated by the magnet coil currents, time varying (RF) currents, and the steady state plasma: $\boldsymbol{B}(r, f, z, t) = \boldsymbol{B}_0(r, z) + \boldsymbol{B}_{RF}(r, f, z, t) + \boldsymbol{B}_p(r, z)$. The electric field is a sum of the time varying (RF) electric field and steady state field produced by the plasma: $\boldsymbol{E}(r, f, z, t) = \boldsymbol{E}_{RF}(r, f, z, t) + \boldsymbol{E}_p(r, z)$. In general, there is also the possibility of an applied steady state bias field, but it is not considered in the present system. Here, r, f, z represent the radial, azimuthal and axial coordinates in a cylindrical coordinate system, and t represents time. In the article we use a bold font for the vector variables. All equations are written in SI units.

The calculations for VASIMR currently incorporate six integrated models for calculation of these fields as shown in Figure 2. More details for each of the physics models used in these calculations are given in later sections. The calculation proceeds as follows (see Figure 2).

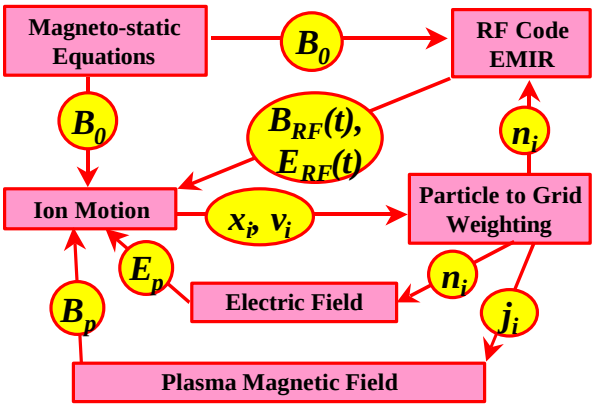

Figure 2: Mathematical simulation of plasma in VASIMR

First, the magnetostatic field produced by the magnet coils, $\boldsymbol{B}_0(r, z)$, is accurately generated. This field does not change throughout the remaining calculation.

Second, the RF fields, $\boldsymbol{E}_{RF}(r, f, z, t)$ and $\boldsymbol{B}_{RF}(r, f, z, t)$, are calculated using a Maxwell equation solver with a linearized cold plasma conductivity tensor and $\boldsymbol{B}_0(r, z)$. Damping in the cold plasma model is provided by a single de-correlation parameter and plasma density, $n(r, z)$, which are initially assumed. The de-correlation parameter adjusts the absorption and electric field profile near the first harmonic ion resonance in the plasma.

Third, a fully nonlinear particle model, that is currently collisionless, calculates the ion positions and velocities $\boldsymbol{x}_i(t)$, $\boldsymbol{v}_i(t)$ based on Newton's law using the Lorentz force calculated from the static and RF fields obtained from the Maxwell equation solvers in a three-dimensional space.

Fourth, the ion density, $n_i(r, z)$ and ion current density $\boldsymbol{j}_i(r, z)$ are calculated from the ion positions and

velocities averaging over the gyro-motion, using a particle to grid weighting. The resulting ion density is approximately equal to the electron density in a quasineutral approximation, and it is fed back into to the plasma conductivity tensor for the next iteration with the RF Maxwell equation solver. The iteration is continued between these two models until the plasma density becomes constant. Presently, in lieu of a fully nonlinear RF plasma response, the iteration process proceeds further by adjusting the de-correlation parameter in the cold plasma dielectric, and hence the field pattern near resonance, until the power absorbed by the ions in each model converges

The fifth step iterates over the previous models using $n_i(r, z)$ and a Boltzmann approximation for the electron distribution to solve Poison's equation for the steady state plasma potential giving $\boldsymbol{E}_p(r, z)$. This field further modifies the plasma density and hence the RF coupling.

The steady state plasma current density, $\boldsymbol{j}_i(r, z)$ becomes important in the exhaust region where $\boldsymbol{B}_p(r, z)$ can become significant compared with the fields from the magnet coils. Thus, the sixth and final step calculates steady state magnetic field corrections caused by the plasma in the exhaust region.

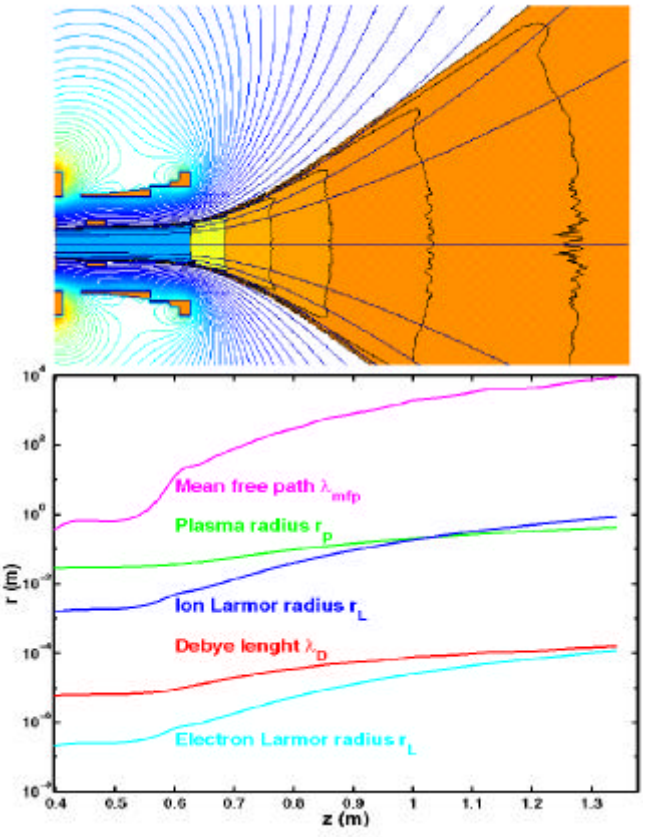

Figure 3. Scale lengths of 10 kW VASIMR thruster.

The approximations and basic physics parameters used in the models can be justified for a low power VASIMR device as shown in Figure 3. The Debye length l_D is much less than plasma radius r_p which makes the assumption of plasma quasi-neutrality good everywhere except in very localized sheath regions. Although collisional processes can play an important role in the plasma source region, the plasma can be assumed reasonably collisionless in the central section so long as the mean free path l_{mfp} for various collision processes is much larger than plasma dimensions. The following of only the ion species in the particle simulation can be justified by the fact that electrons are attached to the magnetic field through most of the region of interest, and gyrate with a frequency much higher than the applied RF frequency for the system. Ions are normally attached to the magnetic field inside the thruster and the beginning of the exhaust area. However, they detach at distance of $1m$ from the thruster when the ion Larmor radius r_L^i becomes larger than the magnetic field curvature. The plasma currents generated in the exhaust region will allow the entire plasma to detach in either a stable MHD equilibrium or quasistatic turbulent state.

In the mathematical model of the magnetoplasma thruster, the body of the rocket, the power plant and other hardware is assumed not to affect the electric and magnetic fields of the thruster and hence excluded from the consideration.

1) Magnetostatic Equations.

The magnetostatic problem is a steady-state case of two vector Maxwell equations:

$$\nabla\times\frac{1}{m}\boldsymbol{B}_0=\boldsymbol{j}_0,\qquad \boldsymbol{B}_0=\nabla\times\boldsymbol{A}_0, \tag{1}$$

where $\boldsymbol{B}_0$ is the vacuum magnetic induction vector, μ is the magnetic permeability, $\boldsymbol{j}_0$ is the current density in electromagnets and $\boldsymbol{A}_0$ is the magnetic vector potential. When modeling the VASIMR system, the assumptions of cylindrical symmetry and constant magnetic permeability μ are valid. In that case, the magnetic vector potential $\boldsymbol{A}_0$ (as well as current density vector $\boldsymbol{j}_0$), written in the cylindrical coordinate system (r, f, z), has only an azimuthal nonzero component: $\boldsymbol{A} = (0, A_f(r, z), 0)$ and the problem (1) can be rewritten in the following form:

$$-r\frac{\partial}{\partial r}\frac{1}{r}\frac{\partial F}{\partial r}-\frac{\partial^2 F}{\partial z^2}=f(r,z)=mrj_0,\ (r,z)\in W, \tag{2}$$

where $F(r, z) = r A_f(r, z)$ is the magnetic flux.

Equation (2) is solved together with homogeneous boundary conditions $F = 0$ at the symmetry line ($r = 0$) and at the computational domain boundary, located far

enough from the current source ($r = 10$ m, $z = \pm 10$ m). The finite difference method is used for discretizing of equation (2) using a non-uniform mesh, adapted to the coil geometries and computational domain:

$$Dz_{j-1/2}\left[\frac{F_{ij}-F_{i-1,j}}{r_{i-1/2}Dr_{i-1}}+\frac{F_{ij}-F_{i+1,j}}{r_{i+1/2}Dr_i}\right]+$$
$$+\frac{Dr_{i-1/2}}{r_i}\left[\frac{F_{ij}-F_{i,j-1}}{Dz_{j-1}}+\frac{F_{ij}-F_{i,j+1}}{Dz_j}\right]= \quad (3)$$
$$= Dr_{i-1/2}Dz_{j-1/2}f_{ij};\ i = 2,...,N_r\text{-}1;\ j = 2,...,N_z\text{-}1$$
$$\ddot{O}_{ij} = 0,\ \ i = 1 \ \ or\ N_r \ \ or\ \ j = 1 \ \ or\ N_z$$

The finite difference scheme (3) has a second order of approximation for the "smooth" non-uniform mesh, i.e. when $\frac{Dr_{i-1}-Dr_i}{Dr_{i-1}Dr_i}$ and $\frac{Dz_{j-1}-Dz_j}{Dz_{j-1}Dz_j}$ are bounded. The resulting system of linear algebraic equations is solved by efficient iterative solver[10].

Since equation (2) is linear it can be solved for the each single coil separately, which gives less computational error for the same number of grid points. Then the final magnetic induction solution is calculated by superposing the single coil solutions and interpolating.

Figure 1 demonstrates the numerical solution for the vacuum magnetic field for a 10 kW VASIMR thruster. As numerical experiments show, to calculate magnetic field with less than *0.1%* error, one needs to use a non-uniform mesh with *200* x *500* mesh points. The accuracy of the numerical solution can be estimated by using the known semi-analytical solution of the magnetic field on the symmetry line.

2) ICRF Electromagnetic Field Calculation

In the EMIR code[11], the RF electric field, $\boldsymbol{E}_{RF}$, magnetic field, $\boldsymbol{B}_{RF}$, and RF antenna current density, $\boldsymbol{j}_{RF}$, are expanded in a periodic Fourier sum in the azimuthal coordinate to reduce the three-dimensional problem to a weighted sum over two-dimensional solutions. Implicit time dependence of e^{-iwt} is assumed as well as azimuthal symmetry of the equilibrium quantities, so that the fields and currents can be expanded into azimuthal modes:

$$\boldsymbol{E}_{RF}(r,f,z,t) = \sum_m \boldsymbol{E}_m(r,z)e^{imf-iwt}, \quad (4)$$

where m is an azimuthal mode number and w is RF frequency.

The RF fields are obtained from the EMIR code by solving Maxwell's equations, written in harmonic form:

$$-\nabla\times\nabla\times\boldsymbol{E}_{RF}+\frac{w^2}{c^2}(\boldsymbol{E}_{RF}+\frac{i}{we}\boldsymbol{j}_p) = -iwm\boldsymbol{j}_{ANT}, \quad (5)$$

$$\nabla\times\boldsymbol{E}_{RF} = iw\boldsymbol{B}_{RF}. \quad (6)$$

In the current EMIR implementation, the plasma current density $\boldsymbol{j}_P$ is related to the electric field by a collisional cold plasma conductivity tensor $\boldsymbol{j}_p = \hat{s}\cdot\boldsymbol{E}_{RF}$ with collisional de-correlation. Equation (5) can then be represented by system of independent equations with respect to $\boldsymbol{E}_m$:

$$-e^{-imf}\nabla\times\nabla\times\boldsymbol{E}_m e^{imf}+\frac{w^2}{c^2}\hat{\hat{\boldsymbol{E}}}\cdot\boldsymbol{E}_m = -iwm\boldsymbol{j}_m, \quad (7)$$

where $\hat{\boldsymbol{K}} = \boldsymbol{I}+\frac{i}{we}\hat{s}$ is a cold plasma dielectric tensor:

$$\hat{\boldsymbol{K}} = \begin{pmatrix} K_\perp & -iK_x & 0 \\ iK_x & K_\perp & 0 \\ 0 & 0 & K_{||} \end{pmatrix}$$

and $\boldsymbol{j}_m$ is the current density externally applied by an antenna. The entries of the dielectric tensor depend on the plasma density n_i and the vacuum magnetic field B_0 and the driven frequency w for a multiple-ion plasma as follows:

$$K_\perp = 1-\sum_{l=e,i}\frac{w_{pl}^2}{w^2-w_{cl}^2},\ \ K_x = \sum_{l=e,i}\frac{w_{ci}}{w}\frac{w_{pl}^2}{w^2-w_{ci}^2},$$
$$K_{||} = 1-\sum_{l=e,i}\frac{w_{pl}^2}{w^2},\ \ w_{pl}^2 = \frac{e^2n_l}{e_0m_l},\ \ w_{cl} = \frac{eB_0}{m_l}.$$

where the sum is over the electrons and all ion species. Absorption is introduced in the cold plasma model by adding an imaginary de-correlation frequency to the RF driven frequency, which is equivalent to adding an imaginary particle mass in the dielectric tensor elements.

Because the conductivity along magnetic field lines in the plasma is so large compared with the conductivity in other directions, the parallel plasma current effectively shorts out the component $\boldsymbol{E}_{||RF}$ that is parallel to $\boldsymbol{B}_0$. The solution of Maxwell's equations is considerably simplified by neglecting this parallel field component (but not the parallel current) giving a relation between axial and radial components of $\boldsymbol{E}_{RF}$:

$$E_z = -B_{0z}E_r/B_{0z}. \quad (8)$$

The final system of equations for E_r and E_f has the following form

$$\frac{\partial^2 rE_r}{\partial z^2}+\frac{r}{R}\frac{\partial^2 arE_r}{\partial r\partial z}+\left(\frac{w^2}{c^2}K_\perp-\frac{m^2}{r^2}\right)\frac{rE_r}{B_{0z}^2}+$$
$$+\frac{a}{R}\left(r\frac{\partial^2 rE_r}{\partial r\partial z}+\frac{r}{R}\frac{\partial}{\partial r}r\frac{\partial arE_r}{\partial r}+im\frac{\partial rE_f}{\partial z}\right)- \quad (9)$$
$$-i\frac{w^2}{c^2}\frac{K_x}{B_{0z}}rE_f-\frac{im}{r}\frac{\partial rE_f}{\partial r}=-iwmr\left(j_{r,m}-\frac{ar}{R}j_{z,m}\right),$$
$$r\frac{\partial}{\partial r}\left(\frac{1}{r}\frac{\partial rE_f}{\partial r}\right)+\frac{\partial^2 rE_f}{\partial z^2}+\frac{w^2}{c^2}K_\perp rE_f-\frac{im}{R}\frac{\partial arE_r}{\partial z}+ \quad (10)$$
$$+i\frac{w^2}{c^2}\frac{K_x}{B_{0z}}rE_r-imr\frac{\partial}{\partial r}\left(\frac{E_r}{r}\right)=-iwmrj_{f,m},$$

where $a=B_{0r}R/(B_{0z}r)$, R is the radius of a perfectly conducting wall boundary. Boundary conditions for equations (9, 10) are derived from the property, that the tangential component of $\boldsymbol{E}_m$ vanishes on the boundary $r = R$, and $z = 0, L$. This gives $E_r = E_f = 0$ at $z = 0, L$ and at $r = R$. In the discretization, Equations (9) and (10) are solved with respect to the dependent variables rE_r and rE_f.

The power coupled to the plasma must equal the power emitted by the antenna according to Poynting's theorem

$$\int_V \frac{1}{2}Re[\boldsymbol{E}_{RF}\cdot(\boldsymbol{j}_p+\boldsymbol{j}_{ANT})^*]dV+\oint_{\partial V}Re(\boldsymbol{S}\cdot\boldsymbol{n})d(\partial V)=0,$$

where $\boldsymbol{S} = (\boldsymbol{E}_{RF} \times \boldsymbol{B}_{RF}^*)/(2m_0)$ is the complex Poynting vector and $\boldsymbol{n}$ is the unit vector normal to the integration surface. Taking the volume of integration over the perfectly conducting boundary eliminates any contributions from the Poynting flux through the boundaries. Using the conductivity tensor to calculate the plasma current and evaluating the volume integral gives the total power absorbed by the plasma for a known antenna current. Convergence of the difference scheme can be measured by calculating the power generated by the antenna and comparing it with the absorption in the plasma.

The RF power absorption by the plasma for a known antenna current determines the plasma loading resistance, which is a very important parameter for an antenna design. In a lumped circuit model, the resistance for each antenna segment can be defined as twice the power emitted by that segment divided by the square of the current in that segment. To efficiently couple RF power, the plasma loading resistance for the entire antenna must be substantially larger that the vacuum loading resistance which is caused by finite resistance effects throughout the entire circuit driving the antenna.

In many cases, good antenna designs permit a reasonably accurate solution using just one major mode m. For more accurate calculations, several m modes are used and the system (9, 10) is be solved independently for each m, and the final solution in real space is obtained by summing over the modes.

In Figure 4 we show the RF electric field amplitudes and absorbed power for the $m = -1$ mode ($m = 1$ for the opposite magnetic field direction) propagating from the antenna to a magnetic beach, where w is equal to the ion gyro-frequency. The $m = -1$ mode penetrates to the axis with the correct polarization to accelerate ions in the direction perpendicular to the static magnetic field. A good antenna design for the ICRF section will excite primarily the $m = -1$ mode and produce a loading resistance that is high enough for the desired power of 6-8 kW to be coupled by the RF feed system, matching network, and transmitters.

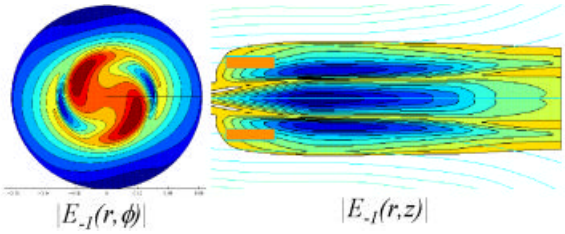

Figure 4. Contours of the electric field component having the proper polarization for ion absorption for $m = -1$.

3) Particle Dynamics.

The ion motion satisfies the following equation of motion:

$$m_i\frac{d\boldsymbol{v}_i}{dt}=e(\boldsymbol{v}_i\times\boldsymbol{B}+\boldsymbol{E}). \quad (11)$$

The single particle trajectories are integrated from equation (11) with an adaptive time-scheme, which can quickly solve extensive particle simulations for systems of hundreds of thousands of particles in a reasonable time (1-2 hours), and without the need for a powerful supercomputer.

The particle motion problem (11) can be rewritten in the form

$$m_i\frac{d\boldsymbol{v}_i}{dt}=f_i(t,\boldsymbol{x}_i,\boldsymbol{v}_i) \quad (12)$$

and can be solved efficiently by the semi-explicit scheme, often referred to as leap-frog[4]:

$$\boldsymbol{x}^{n+1/2}=\boldsymbol{x}^{n-1/2}+Dt^n\boldsymbol{v}^n,$$
$$\boldsymbol{v}^{n+1}=\boldsymbol{v}^n+Dt^n f_i\left(t^{n+1/2},\boldsymbol{x}^{n+1/2},\frac{\boldsymbol{v}^n+\boldsymbol{v}^{n+1}}{2}\right) \quad (13)$$

The scheme has a second order, when $\frac{Dt^{n+1} - Dt^n}{Dt^n}$ is bounded. Numerical experiments show that the method described above conserves the kinetic energy of the particle $W_i = \frac{m_i v_i^2}{2}$ for the magnetostatic case, while the first order explicit scheme does not.

Particles in the electro-magnetic field have oscillated spiral-shaped trajectories with corresponded Larmor radius $r_L = \frac{m_i v_\perp}{eB}$ and Larmor period $t_L = \frac{2pm_i}{Be}$. Since the magnetic induction B is very nonuniform, the Larmor period can have very wide range of values. To reduce the trajectory calculation time without reducing the accuracy, it is reasonable to choose non-uniform time step to be proportional to the Larmor period:

$$Dt = \frac{t_L}{N_t}, \qquad (14)$$

where N_t is a number of the time steps per Larmor period. In most of our simulations we choose $N_t = 100$.

Figure 5 illustrates magnetic field lines and typical ion trajectories in the exhaust area of the VASIMR. One can see the beginning of the particle detachment from the magnetic field in the exhaust area with weak magnetic field. Since the magnetic flux Br_p^2 is a constant, where r_p is a plasma radius, the magnetic field goes down as fast as r_p^{-2}. Since the magnetic moment $\frac{m_i v_\perp^2}{2B}$ is approximately constant, the perpendicular velocity $v_\perp$ goes down as fast as r_p^{-1}. This makes the Larmor radius r_L go up as fast as r_p.

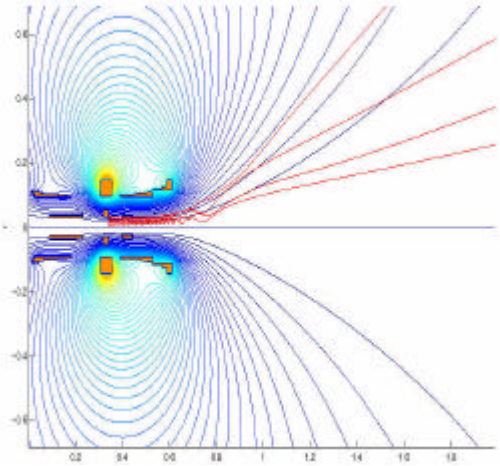

Figure 5. Magnetic field lines and test ion trajectories in the VASIMR. Four trajectories with the same initial velocity but different radial position are observed.

Figure 6 demonstrates the behavior of the axial and parallel (to the magnetic field) velocities for test particles from Figure 5.

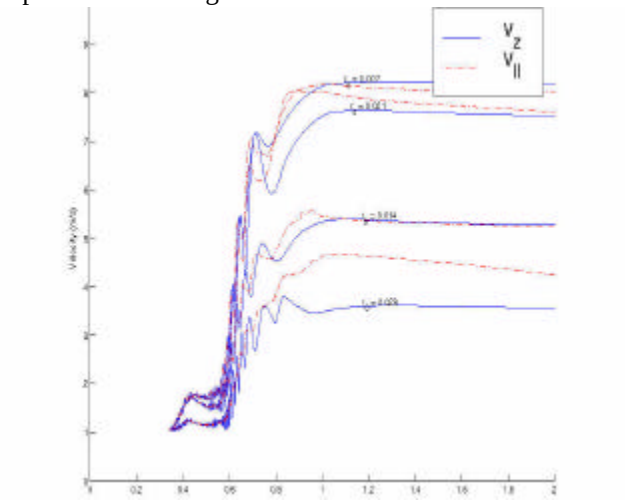

Figure 6. Axial (solid line) and parallel to the magnetic field (dashed line) velocity propagation for the test ion trajectories shown at Figure 5.

One can see that parallel velocities reach a maximum and then go down as the magnetic field line departs from the ion trajectory, which illustrates the effect of plasma detachment. The axial velocity, which is responsible for the directed thrust of the rocket, approaches an asymptotic value, which also demonstrates detachment. The efficiency of the ICRF can be quantitatively estimated by the ratio of the final total axial velocity of the ions to the initial total velocity. The ratio is much larger than one (around 3), thus increasing the directed ion energy by factor 9.

4) Particle to Grid Weighting

The ion density n_i is calculated by using weighting method[4] for method of trajectories[8]. With a given distribution for the initial position and velocity vector, a big number (order of 10^5) of ion trajectories is calculated. Every single trajectory is used to generate a number of particles distributed along it with equal time step between them. Plasma density clouds with a certain weight and a size of the finite difference cells are produced around each particle point, which after summation, became discrete ion density n_i defined constant at each finite difference cell, using the following formula

$$n_i(\boldsymbol{X}_j) = w_i \sum_k Q(\boldsymbol{X}_j - \boldsymbol{x}_k),$$

where $\boldsymbol{X}_j$ is a position of the j-cell, x_k is a position of k-particle, w_I is a particle weight, $Q(.)$ is a cloud density function. In our simulation we used continuous piece-

wize-linear function with a support equal shape of the j-cell. The particle weight w_i is calculated, such that it makes the grid density equal given value at given point:

$$n_i(\boldsymbol{X}_0) = n_i^0$$

The example of the ion density, calculated by particle method, is shown in Figure 7.

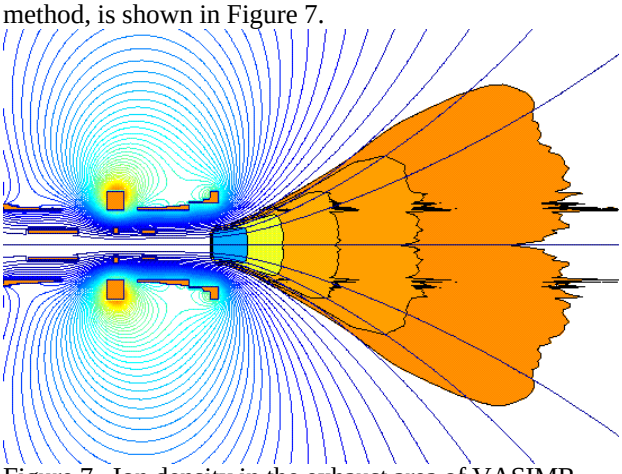

Figure 7. Ion density in the exhaust area of VASIMR.

The similar technique is used to calculate the ion density $\boldsymbol{j}_i$, ion energy W_i, ion energy spread ("temperature") T_i and heat flux of the plasma H_i:

$$\boldsymbol{j}_i(\boldsymbol{X}_j) = e w_i \sum_k Q(\boldsymbol{X}_j - \boldsymbol{x}_k)\boldsymbol{v}_k;$$

$$W_i(\boldsymbol{X}_j) = \frac{m_i}{2}\frac{w_i \sum_k Q(\boldsymbol{X}_j - \boldsymbol{x}_k)\boldsymbol{v}_k^2}{n_i(\boldsymbol{X}_j)};$$

$$T_i(\boldsymbol{X}_j) = \frac{m_i}{2}\frac{w_i \sum_k Q(\boldsymbol{X}_j - \boldsymbol{x}_k)(\boldsymbol{v}_k - \boldsymbol{V}_p(\boldsymbol{X}_j))^2}{n_i(\boldsymbol{X}_j)};$$

$$\boldsymbol{H}_i(\boldsymbol{X}_j) = \frac{m_i}{2} w_i \sum_k Q(\boldsymbol{X}_j - \boldsymbol{x}_k)(\boldsymbol{v}_k \cdot \boldsymbol{v}_k)\boldsymbol{v}_k;$$

To calculate plasma current density accurately, using particle-to-cell weighting method, one needs to choose a cell size less than the Larmor radius. On the other hand, making cells too small forces us to run much more trajectories to keep enough number of particles per cell. To satisfy *1%* accuracy in particle-to-cell weighting method, we need to generate so many trajectories, that the number of particle positions $\boldsymbol{x}_k$ per cell would be of order *10,000*.

5) Electrostatic Equations.

The electric field E_p can be calculated through electric potential $\boldsymbol{j}$:

$$E_p = -\nabla \boldsymbol{j}\ , \qquad (15)$$

which satisfies the following Poisson equation:

$$-D\boldsymbol{j} = e(n_i - n_e), \qquad (16)$$

where the right-hand side is a plasma charge density. To avoid calculation of the electron density function, the Boltzmann relation is used:

$$n_e = n_0 \exp\left(\frac{e\boldsymbol{j}}{kT_e}\right), \qquad (17)$$

where the bulk electron density n_0 is assumed equal the ion density at the plasma inlet (assuming that $\boldsymbol{j}=0$ there), and is a constant function along every magnetic field line.

In the present simulations the electron temperature T_e is assumed constant. Due to the very small value of the Debye length for the studied plasma system:

$$l_D = \sqrt{\frac{kT}{4\pi n e^2}} < 10^{-4}\ \text{m}, \qquad (18)$$

the Poisson equation (16) can be simplified to the quasineutrality relation: $n_i = n_e$, which gives the following formula for the electric potential:

$$\boldsymbol{j} = \frac{kT_e}{e}\ln\left(\frac{n_i}{n_0}\right). \qquad (19)$$

To avoid $\ln(0)$ calculations, the ion density can be adjusted by some small positive constant. Equation (19) has to be solved in the loop with particle simulations for the ions using an updated electric field. To achieve convergence in the self-consistent plasma – electric field calculations, under-relaxation (damping) is needed for updating the electric potential: $\boldsymbol{j}_{new} = \tau \boldsymbol{j}^* + (1-\tau)\boldsymbol{j}_{new}$ with a relaxation parameter $\tau < 1$.

Figure 8 demonstrates the electric potential solution for the plasma system shown at Figure 7. The negative electric potential in the exhaust area generates positive an outcomming electric field, which accelerates ions and increases the VASIMR performance.

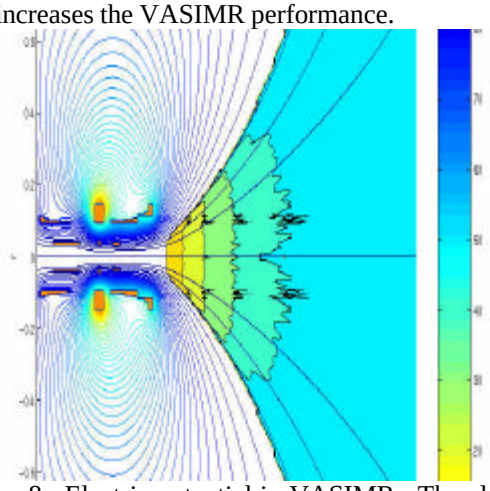

Figure 8. Electric potential in VASIMR. The electric field is solved self-consistently with the plasma density, shown in Figure 7.

6) Calculation of the internal plasma magnetic field

Internal plasma magnetic field can be calculated using the same solver, as used for vacuum magnetic field calculation. The only different in this calculation is a current density source $\boldsymbol{j}_p$. The calculation of $\boldsymbol{B}_p$ should be iterated with calculation of plasma velocity and density.

As numerical experiments show, the internal plasma magnetic field in the thruster core has an opposite direction to the vacuum magnetic field. In the exhaust area, when ions detach from the vacuum magnetic field, the internal plasma magnetic field has the same direction. In either case, the internal plasma magnetic field is thousands time less than vacuum magnetic field for the studied range of plasma parameters.

OBSERVATION OF ICRF HEATING

Particle simulation in VASIMR demonstrates dramatic increase in perpendicular velocity of ions as they pass through the ion-cyclotron resonance area. Further down stream, the orthogonal energy of the particles is converted into directed parallel energy due to the decrease of the magnetic field in the magnetic nozzle (Figure 9.)

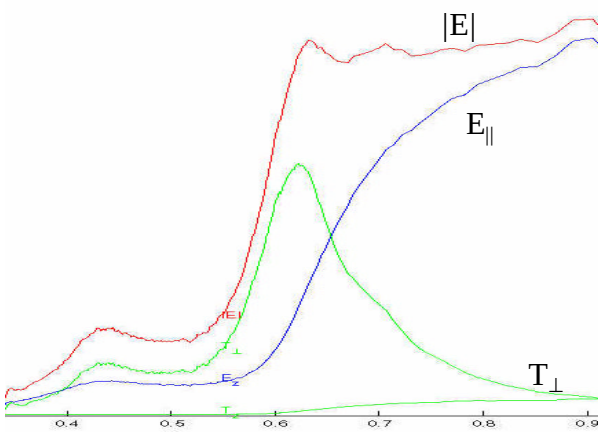

Figure 9. Plasma energy and temperature propagation on a symmetry line as a result of RF-heating and magnetic nozzle.

To obtain a reasonably self-consistent picture of the ICRH absorption (Figure 10,) the ion trajectories are followed through the static and RF fields using the trajectory code VASIMR. The iteration is performed by calculating the RF fields with the EMIR code, and using these fields to follow nonlinear ion trajectories with the VASIMR code on the gyro-frequency time scale. The ion trajectories are used to generate RF power absorption values and a density input for the next EMIR calculation. The codes are iterated until the density profile becomes reasonably stable, then the collisional absorption parameter in the EMIR code is adjusted and the iteration is continued until the power deposited by the RF system matches the power absorbed by the ion trajectories in a global sense.

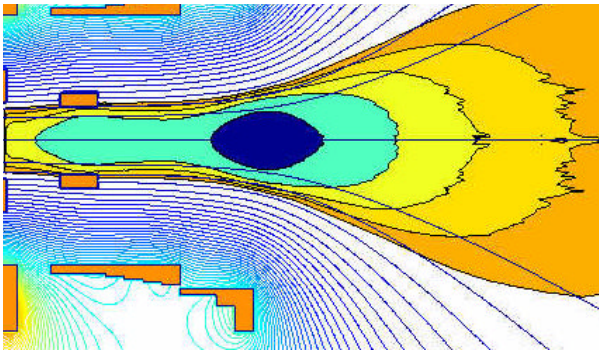

Figure 10: RF power deposition contours

The total power delivered by the RF amplifier is equal to the power delivered to the plasma, P_p, plus that dissipated by Joule heating in the circuit, P_c. An efficiency for the delivery of RF power to the plasma can thus be defined as:

$$h = \frac{P_p}{P_p + P_c} = \frac{r_p}{r_p + r_c},$$

where r_p and r_c are the effective loadings by the plasma and circuit respectively.

For Helium plasma densities in the range of $1 - 2 \times 10^{19}$ in the 10 kW thruster design, preliminary antenna designs in the model appear capable of achieving values of r_p around 300 milliOhms for each of the two phased array segments. The vacuum loading of the circuit, r_c, will depend on the details of the feed system, but it is expected to be much lower than 300 milliOhms. A typical goal for the circuit design might be less than 50 milliOhms giving an RF power delivery efficiency, $h \sim 85\%$. This level of efficiency for the power transmission is probably acceptable, but higher values of r_p and lower values of r_c are clearly desirable.

CONCLUSION

The described particle simulations in VASIMR demonstrate ion heating by ICRF waves and detachment from the nozzle. The codes developed so far have already been used to help VASIMR researchers design an experimental ICRF antenna.

In the future, we plan to make our simulation technique more advanced and closer to the reality of the physical system. This effort will involve implementing the following physical effects: 1) calculate the electron temperature as a function of space using information about neutral particles in the system; 2) calculate the internal plasma current through the plasma momentum stress tensor, which will cause magnetic field distortion in the nozzle region, 3) add Monte-Carlo collision operators to study the effects of charge exchange on the accelerated ions and the heat loads from such a particle flux on the antenna and rocket body, 4) benchmark loading results with experimental measurements, and look for inconsistencies with the model's assumptions, 5) evolve more efficient antenna designs to improve plasma loading, 6) study turbulent effects in the plasma nozzle region, and 7) add more consistent nonlinear local feedback between the particle solution and the RF Maxwell solver.

NOMENCLATURE

A	magnetic potential (Weber / m)
B	magnetic induction ($0 - 1$ Tesla)
c	speed of light ($3\ 10^8$ m / s)
E	electric field (Volt / m)
e	electron charge ($1.6\ 10^{-19}$ Coulomb)
F	thrust ($0.1 - 0.2$ N)
f	right-hand side in the magnetostatic equation
H	heat flux ($0\text{-}10^6$ W / m^2)
$\boldsymbol{I}$	identity tensor
I_{sp}	specific impulse ($5000 - 10^4$ s)
i	imaginary unit
j	current density ($0 - 10^5$ Ampere / m^2)
k	Boltzmann constant ($1.38\ 10^{-23}$ J / K)
kT_e/e	electron temperature ($1 - 10$ electron-Volt)
kT_i/e	ion temperature ($10 - 100$ electron-Volt)
L	plasma length (0.5 m)
M	VASIMR mass ($20 - 100$ kg)
m	particle mass (He ion: $6.68\ 10^{-27}$ kg)
$\dot{m}$	propellant flow rate (10^{-6} kg/s)
N_r, N_z	mesh size (200×500)
N_t	time-step factor (100)
n	density ($0 - 10^{19}$ m^{-3})
$\boldsymbol{n}$	normal-to-surface vector
P	power (10^4 Watt)
Q	particle cloud function
R	radius of a boundary metal wall (m)
r, f, z	cylindrical coordinates (radial, azimuthal and axial)
r_L	Larmor radius ($10^{-2} - 1$ m)
r_p	plasma radius ($0.02 - 0.1$ m)
$\boldsymbol{S}$	Poynting vector
t	time (s)
u	exhaust velocity (10^4 - 10^5 m/s)
V	plasma volume (m^3)
v	particle velocity (ion: $10^4 - 10^5$ m / s)
W	energy (J)
w	particle cloud weight
$\boldsymbol{X}$	cell position (m)
$\boldsymbol{x}_i$	ion 3-D position vector (m)
a	coefficient in harmonic RF equation
Dr_i, Dz_j	grid sizes
Dt^n	time step size
∂V	edge of the volume
e	power efficiency (0.5)
F	magnetic flux (Tesla m^2)
j	electric potential (-100 - $+10$ Volt)
h	RF efficiency
$\hat{K}$	cold plasma dielectric tensor
l_D	Debye length ($10^{-4} - 1$ m)
l_{mfp}	ion mean free path ($10^0 - 10^3$ m)
m	magnetic permeability ($1.25\ 10^{-6}$ Henry / m)
p	3.14159265358
r	loading (300 milliOhm)
$\hat{s}$	cold plasma conductivity tensor (Siemens / s)
W	computational domain
w	RF frequency ($7\ 10^6$ - $1.4\ 10^7$ Hz)

Subscripts:

0	vacuum
ANT	ICRF antenna
c	cyclotron (gyro-)
e	electron
i	ion
j	cell
i,j	grid index
k	particle
L	Larmor
l	species index
m	mode number
n	time step
p	plasma
RF	radio-frequency
$\wedge$	orthogonal to vacuum magnetic field $\boldsymbol{B_0}$
$\|\|$	parallel to vacuum magnetic field $\boldsymbol{B_0}$

ACKNOWLEDGMENTS

This research was sponsored by NASA L. Johnson Space Center. Authors thank Roger Bengtson and Alexey Arefiev (University of Texas at Austin), Kim Molvig and Oleg Batishchev (MIT), Roald Sagdeev and Sergey Novakowskii (University of Maryland) and Rick Goulding (Oak Ridge National Laboratory) for useful comments and suggestions.

REFERENCES

1. Chang Díaz F.R., "Research Status of The Variable Specific Impulse Magnetoplasma Rocket", *Proc. 39th Annual Meeting of the Division of Plasma Physics* (Pittsburgh, PA, 1997), *Bulletin of APS*, **42** (1997) 2057.

2. Chang Díaz, F. R. "Research Status of The Variable Specific Impulse Magnetoplasma Rocket", *Proceedings of Open Systems' July 27-31, 1998*, Novosibirsk, Russia, American Nuclear Society, *Transactions of Fusion Technology*, **35** (1999) 87-93.

3. Chang Díaz, F. R., Squire, J. P., Ilin, A. V., et al. "The Development of the VASIMR Engine", *Proceedings of International Conference on Electromagnetics in Advanced Applications (ICEAA99), Sept. 13-17, 1999*, Torino, Italy, (1999) 99-102.

4. Birdsall, C. K. and Langdon, A. B. *Plasma Physics Via Computer Simulation*, Inst. of Physics Publishing, Bristol UK, (1995) 479.

5. Boyd, I. D., Keidar, M., and McKeon, W. "Modeling of a Plasma Thruster From Plasma Generation To Plume Far Field", *Proceedings of 35-th Joint Propulsion Conference, June 20-24, 1999*, Los Angeles, CA, AIAA-99-2300 (1999) 23.

6. VanGilder, D. B., Keidar, M., and Boyd, I.D. "Modelling Hall Thruster Plumes Using Particle *Proceedings of 35-th Joint Propulsion Conference, June 20-24, 1999*, Los Angeles, CA, AIAA-99-2294 (1999) 12.

7. Wang, J., Anderson, J., and Polk, J. "Three-Dimensional Particle Simulation of Ion Optics Plasma Flow", *Proceedings of 34-th Joint Propulsion Conference, July 13-15, 1998, Cleveland, OH*, AIAA-98-3799 (1998) 11.

8. Ilin V.P. *Numerical Methods for Solving Problems in Electrophysics*, (in Russian) Nauka, Moscow (1985) 335.

9. Chang Díaz F. R., et al., "Rapid Mars Transits With Exhaust-Modulated Plasma Propulsion", *NASA Technical Paper* 3539, (1995).

10. Ilin, A. V., Bagheri, B., Scott, L. R., Briggs, J. M., and McCammon, J. A. "Parallelization of Poisson-Boltzmann and Brownian Dynamics calculation", *Parallel Computing in Computational Chemistry*, ACB Books, Washington D.C., (1995) 170-185.

11. Jaeger E.F., Batchelor D.B., Weitzner H. and Whealton J.H. "ICRF Wave Propugation And Absorption in Tokamak And Mirror Magnetic Fields – A Full-wave Calculation", *Computer Physics Com.*, **40** (1986) 33 – 64.

12. Hockney, R. W., and Eastwood, J.W., *Computer Simulation Using Particles*, Inst. of Physics Publishing, Bristol UK, (1988).

13. Ilin A.V., Chang Díaz F.R., Squire J.P. and Carter M.D. "Monte Carlo Particle Dynamics in a Variable Specific Impulse Magnetoplasma Rocket", *Proceedings of Open Systems' July 27-31, 1998*, Novosibirsk, Russia, American Nuclear Society, *Transactions of Fusion Technology*, **35** (1999) 330 – 334.